Results in Physics 82 (2026) 108590

Contents lists available at ScienceDirect

Results in Physics

journal homepage: www.elsevier.com/locate/rinp

Localization–delocalization transition in the Generalized Aubry–André–Harper Model in a quasiperiodic superlattice potential

Zain Ullah [b], Muhammad Sajid [c], Amsyar Rahim [b], Mohd Faudzi Umar [d], Nurisya Mohd Shah [a,b,*]

[a] Institute for Mathematical Research, Universiti Putra Malaysia, 43400 UPM Serdang, Selangor Darul Ehsan, Malaysia
[b] Department of Physics, Faculty of Science, Universiti Putra Malaysia, 43400 Serdang, Selangor Darul Ehsan, Malaysia
[c] Department of Physics, Kohat University of Science and Technology, Kohat, 26000, Khyber Pakhtunkhwa, Pakistan
[d] Department of Physics, Faculty of Science and Mathematics, Universiti Pendidikan Sultan Idris, 35900 Tanjong Malim, Perak, Malaysia

ARTICLE INFO

Keywords:
Quantum transport
Quasiperiodic systems
Localization
Topological phenomena

ABSTRACT

We investigate localization–delocalization transition in the one-dimensional generalized Aubry–André–Harper (GAAH) model in a quasiperiodic superlattice potential. The critical interplay between the model's two modulated energy scales — the hopping amplitude (t) and the on-site potential (Δ) — generates a rich phase diagram featuring extended, localized, and critical phases. We employ both static spectral and dynamics indicators to identify these phases. In static analysis, we compute the energy spectrum as a function of the common phase ϕ of the modulations and employ the inverse participation ratio (IPR) to map localization–delocalization phase diagram as a function of t and Δ. Dynamically, we model the evolution of an initially localized quantum state as a continuous-time quantum walk (CTQW), analyze the resulting probability distribution and time-dependent IPR to corroborate the static results. This work establishes a direct correspondence between static spectral indicators and dynamics, providing a unified framework for characterizing localization in quasiperiodic systems. Our findings offer new perspectives for controlling quantum transport in engineered quantum platforms.

Introduction

Quasiperiodic systems hold an intermediate regime between perfectly ordered crystalline solids and fully disordered media [1]. These systems exhibit interesting spectral and transport properties that are different compared to conventional extended Bloch states and exponentially localized states. One of the celebrated models in this class is the Aubry–André–Harper (AAH) model, originally introduced in the context of electrons hopping on a two-dimensional (2D) lattice subject to an external magnetic field [2–4]. In the simplest case, this model describes a one-dimensional (1D) tight-binding system with a modulated onsite or hopping potential that offers a convenient platform to investigate transport and topological phenomena [5–8]. For an incommensurate frequency of the modulation, the system makes a sharp transition from extended to localized phase [9–23]. Unlike the Anderson model [24,25], the localization–delocalization transition in the AAH model is deterministic and has been extensively investigated in experiments using various physical platforms [26–34].

Beyond the canonical form, a *generalized* version of Aubry–André–Harper (GAAH) model introduces additional control parameters that results in both on-site and off-diagonal modulations [35]. This modification breaks the exact self-duality of the original AAH model, leading to the emergence of mobility edges that separate localized states from extended states [36–41]. The presence of tunable mobility edges not only enriches the physics of localization but also opens new avenues for controlling quantum transport and interplay with topological properties [42]. Indeed, specific GAAH models have been shown to host nontrivial topological phases, a feature that has been successfully probed in experimental systems [27,29]. Recent experiments with ultracold atoms and photonic waveguide arrays have successfully realized the requisite diagonal and off-diagonal quasiperiodic modulations, firmly establishing the GAAH model as a testbed for these phenomena [43–47].

However, a specific and potent realization of the GAAH model — implemented via an optical quasiperiodic superlattice potential — remains less explored in the context of localization. This particular model incorporates a more complex hopping modulation, characterized by the coexistence of both "Sin" and "Cos" terms, unlike previously

* Corresponding author.
E-mail address: risya@upm.edu.my (N.M. Shah).

https://doi.org/10.1016/j.rinp.2026.108590
Received 23 September 2025; Received in revised form 5 November 2025; Accepted 25 January 2026
Available online 3 February 2026

studied variants. This variant of the GAAH model hosts rich topological phases [48] and could potentially reveal new physics via its interplay with critical or localized phases. A systematic investigation of how the new added complexity into the GAAH model influences the localization–delocalization transition and the associated mobility edges is worth exploring. This is significant in the context of an interplay between multiple topological boundaries and localization could provide enhanced control over quantum transport.

In this work, we present a comprehensive study of localization–delocalization transition in this specific GAAH model by employing both static and dynamical indicators. In the static analysis, we examine the single-particle energy spectrum as a function of the phase ϕ for various values of t and Δ and compute the IPR across all eigenstates to quantify localization properties and identify the mobility edge. We also compute the IPR averaged over all eigenstates to map a global phase diagram in the $t-\Delta$ plane. For the dynamical analysis, which offer a complementary insight directly accessible in experiments, we simulate the continuous-time quantum walk of an initially localized particle, extracting the time-dependent IPR and tracking the full probability distribution to characterize different transport regimes [49–51]. This dual framework links static spectral diagnostics with real-time propagation dynamics, thereby providing a unified perspective on localization phenomena in the GAAH model. Our findings reveal how the specific form of the hopping modulation in the superlattice potential reshapes the localization–delocalization phase diagram, and creates a distinct critical phase. These findings offer potential strategies for controlling quantum state localization and guiding transport in engineered quantum platforms, i.e., ultra-cold atoms confined in optical superlattices.

The remainder of this paper is organized as follows. In Section "Model and methodology", we introduce the GAAH Hamiltonian and outline relevant parameters. Section "Static analysis" presents the static analysis, including the energy spectrum, the IPR of individual eigenstates used to reveal the presence of mobility edges and the IPR averaged over all eigenstates, which enables us to map the localization–delocalization phase diagram. The dynamical analysis is detailed in Section "Dynamics", where we investigate continuous-time quantum walks (CTQWs) and the time evolution of the IPR to characterize transport behavior. Finally, in Section "Conclusion", we summarize our findings and discuss possible directions for future research.

Model and methodology

We consider a generalized Aubry-André Harper model in 1D that describes the dynamics of a quantum particle in an optical superlattice potential in the tight-binding limit. The Hamiltonian consisting of both the hopping and onsite potentials can be written as [48]:

$$\hat{H} = \sum_m \Big[(t_0 + V_m^{\mathrm{od}})(\hat{c}_m^\dagger \hat{c}_{m+1} + \hat{c}_{m+1}^\dagger \hat{c}_m) + V_m^{\mathrm{d}}\, \hat{c}_m^\dagger \hat{c}_m \Big], \tag{1}$$

with

$$V_m^{\mathrm{od}} = -t_1 \cos(2\pi\beta m + \phi) + t_2 \sin(2\pi\beta m + \phi), \tag{2}$$

and:

$$V_m^{d} = \Delta \cos(2\pi\beta m + \phi + \phi_{rel.}). \tag{3}$$

Here, t_0 is the hopping amplitude, V_m^{od} is the strength of the hopping (off-diagonal) modulation, V_m^d is the strength of the onsite (diagonal) modulation, ϕ is the common phase factor, and $\phi_{rel.}$ is the relative phase between the onsite and hopping modulations. The creation (annihilation) operator $\hat{c}_m^\dagger$ ($\hat{c}_m$) creates (annihilates) a quantum particle at a lattice site with position index m. The superlattice potential described by the above Hamiltonian can be realized in experiments, e.g., based on neutral atoms, by superimposing two laser beams (as schematically shown in Fig. 1): one with short wavelength (λ_1) acting as a primary lattice, and the other with long wavelength (λ_2) acting as a perturbation. The long lattice modulates both the onsite and nearest-neighbor hopping energies. Hence, the integrals t_1, t_2, and Δ are proportional to the potential generated by the laser beam of longer wavelength. A detailed derivation of Eqs. (1)–(3) is given in [48].

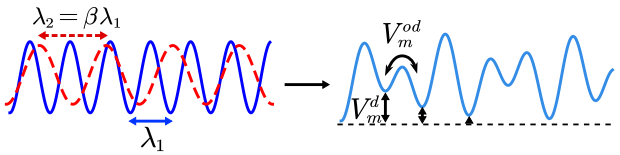

Fig. 1. Schematic of a quasiperiodic superlattice potential generated by superimposing two laser beams of wavelengths λ_1 and λ_2 which are chosen to be incommensurate with each other.

The choice of the modulation frequency $\beta{=}\lambda_2/\lambda_1$ is crucial as it can either result in a periodic potential (for rational values of β) that simulates the dynamic of a quantum system in a perfectly crystalline solid, or a quasiperiodic potential (for an irrational value of β) that simulates an aperiodic system. In this paper, we consider $\beta = \frac{\sqrt{5}+1}{2}$ for which the superlattice potential is shown in Fig. 1. In this case, the model Hamiltonian (Eq. (1)) lacks translation symmetry for any translational operator. However, by an analogy with the 2D Harper Hamiltonian [2,3], the energy dispersion of this Hamiltonian can be studied by treating the phase ϕ as a quasimomentum in the direction perpendicular to the lattice. For the convenience of our analysis in the following sections, we consider $t_0 = 1$, $t_1 = t_2 = t$, and work with dimensionless units. We set the lattice constant, the unit of energy, and the reduced Planck's constant $\hbar$ equal to 1.

To investigate the nature of our model system, i.e., whether it is localized, extended, or critical, we first study the dispersion of the energy spectrum and the probability densities associated with the eigenstates of the system. The GAAH model has topological properties and topological edge (TE) states exist in the energy spectrum when computed on an open chain. We therefore, show the probability densities both for TE states and bulk states for a few representative cases. Since, the TE states are always localized with probability densities concentrated at the end points of the lattice, these states can be distinguished from the bulk states. The nature of the system depends on the probability densities of the bulk states, i.e., if a quantum state has probability density concentrated in a small region in the bulk of the lattice then the system is localized and vice versa.

To rigorously characterize a phase diagram that encodes the behavior of all the eigenstates, we use IPR as a diagnostic tool. IPR is a powerful scalar metric for quantifying the spatial extent and localization properties of quantum states. For a quantum particle residing on the 1D lattice, that can be described by a quantum state $|\Psi\rangle = \sum_{m=0}^{N} \psi(m)|m\rangle$ written in the position bases vectors $|m\rangle$, IPR is defined as [52]:

$$\mathrm{IPR} = \frac{\sum_{m=0}^{N} |\psi(m)|^4}{(\sum_{m=0}^{N} |\psi(m)|^2)^2}. \tag{4}$$

This identifies the inverse of the number of lattice sites over which the probability density of the quantum state is significant. The importance of using IPR lies in its distinct scaling with system size L in different phases: in an extended phase, IPR scales as $\sim 1/L$, and hence, it approaches to 0 in the thermodynamic limit. In contrast, in the localized phase, the quantum state is localized over a few lattice sites with IPR $\sim$ O(1). In the critical phase, the IPR scales with system size as $1/L^{\nu}$, with $0 < \nu < 1$. By computing IPR for the whole energy spectrum of the GAAH model for a range of t and Δ values, we can differentiate the extended, the localized and the critical phases.

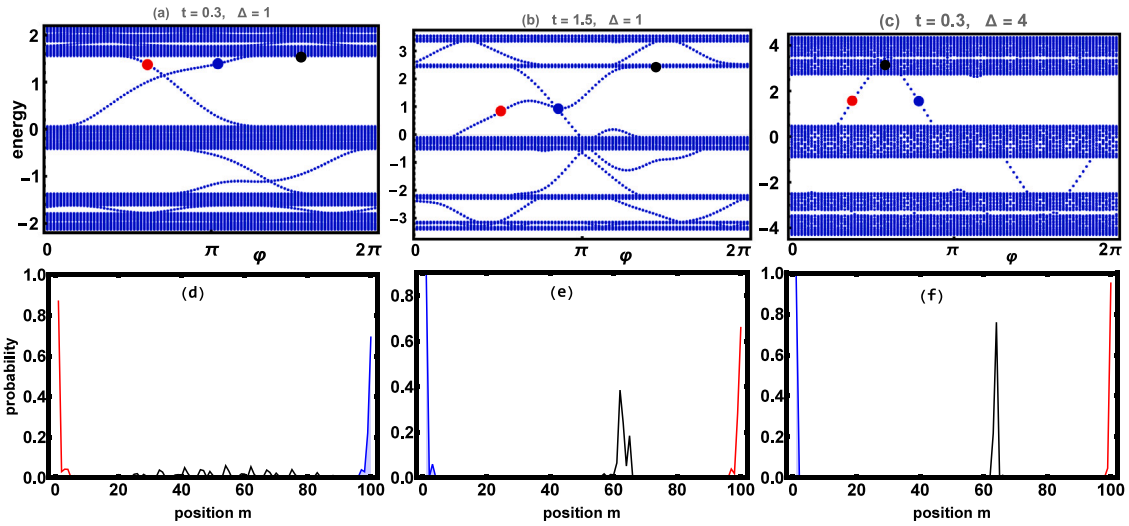

Fig. 2. First row: energy spectrum of the generalized Aubry–André–Harper model under open boundary conditions (OBCs) with parameters (a) (t, Δ)=(0.3, 1), (b) (t, Δ)=(1.5, 1), and (c) (t, Δ)=(0.3, 4). The energy spectrum is asymmetric around $E = 0$ because of broken particle–hole symmetry. The energy spectrum exhibits bulk bands, with TE states traversing the energy gaps. Second row: probability density of three representative eigenstates, i.e., right and left edge states, and a bulk state, chosen from the energy spectrum shown in the first row (filled circles of corresponding colors), same columns. The left and right edge states (indicated by blue and red color, respectively) are localized at the ends of the lattice in all three cases. The bulk state (indicated in black) is extended in (d), with intermediate behavior in (e), and localized in (f). All results are shown for $\phi_{rel.} = 0$.

Static analysis

Energy spectrum

We numerically compute the energy spectrum of the Hamiltonian (Eq. (1)) for the 1D quasiperiodic lattice with open ends. We use three different values for the pair of parameters (t, Δ). The choice of these values will become clear from the localization–delocalization phase diagrams in the next section. The energy spectrum is shown as a function of ϕ in Figs. 2(a)–(c). For these results, the relative phase is fixed at $\phi_{rel.} = 0$. An immediate observation is that the energy spectrum is asymmetric around $E = 0$. This is because of the quasiperiodic modulation of the hopping term that breaks the particle–hole symmetry in the Hamiltonian. In addition to the bulk bands in the energy spectrum, there exist states in the gaps between the bands. These states reflect the non-trivial topological nature of the Hamiltonian.

In Figs. 2(d–f), we plot probability densities of the edge states (indicated by blue and red colors) and bulk states (indicated in black) corresponding to the three cases of Figs. 2(a–c). In each case, the states are selected for specific values of ϕ and energy (indicated by filled circles in the corresponding figures of the first row). These results indicate that the edge states are localized at the corresponding ends of the lattice in all three cases. The probability densities of the bulk states are different for different values of the (t, Δ) pair. As shown, the bulk state in Fig. 2(d) is delocalized over the lattice, in Fig. 2(e) it is localized with a finite spread over a few lattice sites, and in Fig. 2(f) it is completely localized. These results indicate that for the first pair of the control parameters of the Hamiltonian $(t, \Delta) = (0.3, 1)$, the GAAH system is delocalized, for the second pair $(t, \Delta) = (1.5, 1)$, the system has intermediate behavior, and for the third pair $(t, \Delta) = (0.3, 4)$, the system is completely localized.

Localization–delocalization phase diagram

We computed the IPR for all quantum states of our model Hamiltonian (computed under periodic boundary conditions) for various values of the onsite modulation strength Δ. In Fig. 3(a), we show the energy spectrum of the GAAH model as a function of Δ for $\phi = 0$, with a system size of $L = 1000$, $t_0 = 1$, and $t = 0.5$. The values of IPR for each energy eigenstates are overlaid on top of corresponding energies. The IPR values smaller than 0.2 are indicated by blue color and represent extended states. These results show that all eigenstates for $\Delta \lesssim 1.5$ are extended. The IPR values greater than 0.5 are indicated by red color and represent localized states. These states occur at $\Delta \geq 2.5$. Similarly, IPR values between 0.2 and 0.5 are indicated by light blue to yellow colors and represent states with intermediate properties. These occur at $1.5 \leq \Delta \leq 2.5$. These results reveal that the states near the center of the spectrum remain extended up to relatively larger values of Δ, and states close to the edges of the spectrum tend to localize at lower modulation strengths. This energy-dependent localization behavior demonstrates the presence of single-particle mobility edges, i.e., localized and extended states co-exist at a given value of Δ but are separated by critical energies.

To give a global look of the localization–delocalization transition, we compute IPR values for all eigenstates of the Hamiltonian for a range of t and Δ values and average these over eigenstates. Fig. 3(b) shows our results in the $t - \Delta$ plane for $L = 1000$, and $\phi = \phi_{rel.} = 0$. The resulting phase diagram shows three regimes: (i) extended (IPR < 0.2), (ii) localized (IPR > 0.5), and (iii) intermediate ($0.2 \leq$ IPR ≤ 0.5). To investigate whether this intermediate region is a finite-size behavior of the system or represents a stable distinct phase, we analyze the system's size dependence of the IPR. We report these results in Fig. 3(c). The results for the extended and localized regions agree with the expectations, i.e., IPR scales as $\sim 1/L$ in the extended phase and $\sim O(1)$ in the localized phase. Hence, these regions corresponds to stable extended and localized phases. The scaling analysis for the intermediate region clearly shows that its behavior is similar to the localized phase, as the critical exponent of the IPR scaling with L is $\nu = 0.02$ which much closer to the localized phase value $\nu = 0$. We conclude that this intermediate region is a finite-size effect and it is expected to disappear in the thermodynamic limit. The phase diagram then consists of two stable phases, i.e. the extended phase and the localized phase, in the thermodynamic limit.

We repeat these analyses for a non-zero values of $\phi_{rel.}$. We show our numerical results for $\phi_{rel.} = 5.1291$ in Figs. 3(d)–(f). Fig. 3(d) shows the energy spectrum and the energy resolved IPR. The relative phase affects the energy bands structure and shifts the localization transition boundary to higher values of Δ for individual eigenstates. An interesting consequence of including the relative phase is the appearance of a stable "critical" phase as shown in Fig. 3(e). To confirm that it is indeed

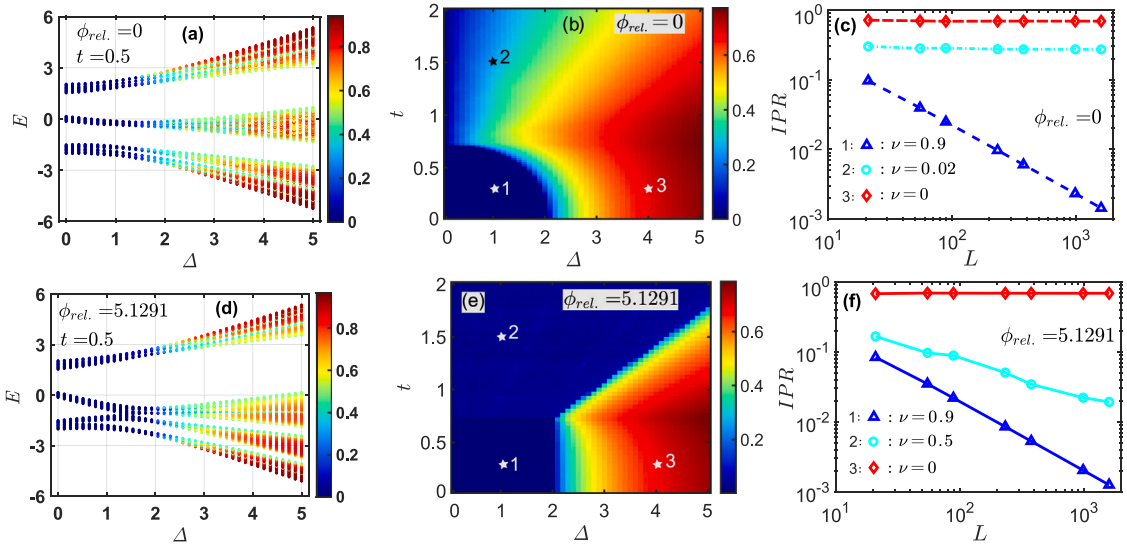

Fig. 3. (a) Energy spectrum of the GAAH model as a function of the diagonal modulation strength Δ, computed for a system size $L = 1000$, $\phi = 0$ and $\phi_{rel.} = 0$ under periodic boundary conditions (PBCs). The IPR values are overlaid (in colors) on top of corresponding energy values which indicate single-particle mobility edges. (b) The global localization–delocalization phase diagram in the $t - \Delta$ plane computed by averaging IPR values over all eigenstates for a range of values of t and Δ. Three regions are visible: the localized region (IPR > 0.5), the delocalized region (IPR < 0.2), and an intermediate region where ($0.2 \leq$ IPR ≤ 0.5). The three pentagrams, labeled by "1", "2", and "3" are the representative points for the extended, intermediate, and localized regions, respectively. (c) Scaling analysis of the IPR with the system size indicates that the intermediate region is a finite size effect and its behavior is resembles the localized phase, i.e., IPR $\propto 1/L^{\nu}$ with $\nu = 0.02$. (d)–(f) Same analysis as shown in the first row but with $\phi_{rel.} = 5.1291$, keeping $\phi = 0$. The intermediate regime in (e) is fully separated from the extended and localized phases. Finite size analysis (f) shows a stable critical phase with IPR $\propto 1/L^{\nu}$, with $\nu = 0.5$ deviating from $\nu = 0$ and $\nu = 1$ which respectively correspond to the localized phase and extended phase.

a stable phase, and its behavior is different from the extended and localized phases, we analyze the IPR as a function of the system size L. The results presented in Fig. 3(f) show that the scaling of IPR with L in the critical region is indeed different, such that it scales as $\sim 1/L^{\nu}$ with $\nu = 0.5$.

The emergence of a critical phase in the localization diagram of the GAAH model has been reported previously [35,45]. In our model, however, the presence of both "Sin" and "Cos" terms in the hopping modulation alters this phase diagram. Specifically, the boundaries between the extended-critical and critical-localized phases are shifted to lower values of t compared to earlier studies [35,45]. It is also important to mention that this phase diagram reflects the system's global behavior, averaged over all eigenstates, unlike the energy-dependent mobility edges shown in Figs. 3(a) and 3(d). For a given parameters set, the assigned phase represents the system's average character, a property we are going to study through dynamical analysis in the following section.

Dynamics

Continuous-time quantum walks (CTQWs) and dynamical IPR on a cyclic lattice

The impact of the onsite and off-diagonal modulations should also be visible in the dynamics of the GAAH system. To investigate these effects in the dynamics, we first consider the time evolution of a continuous-time quantum walk (CTQW) in the bulk of a GAAH cyclic lattice. We consider a quantum particle initially localized at $m = 0$ site of the lattice, i.e. its quantum state can be written as:

$$|\psi(t_e = 0)\rangle = |m = 0\rangle \tag{5}$$

and evolve this state using the GAAH Hamiltonian. The time evolution is governed by the unitary operator generated by the Hamiltonian,

$$|\psi(t_e)\rangle = e^{-i\hat{H}t_e}|\psi(t_e = 0)\rangle. \tag{6}$$

To keep the notation different from the hopping amplitude t, we denote the evolution time by t_e. Since, the Hamiltonian $\hat{H}$ is Hermitian, the evolution operator is unitary and conserves the probability of the quantum state at any instant of time t_e. By computing the quantum state at any instant of time $t_e > 0$ the probability distribution $P(m, t_e)$ across the lattice is computed by projecting the quantum state to the position bases states $|m\rangle$, i.e.,

$$P(m, t_e) = |\langle m|\psi(t_e)\rangle|^2. \tag{7}$$

This allows us to visualize how a quantum particle spreads in space, i.e. whether the wavefunction spreads ballistically, diffusively, or remains localized as the time passes.

In Figs. 4(a)–(c), we show the probability distribution of the quantum particle undergoing a CTQW in the m–t_e plane. We have used three different pairs of parameters (t, Δ), which are indicated with the corresponding results. The common phase ϕ and the relative phase $\phi_{rel.}$ both are set to 0. For $(t, \Delta) = (0.3, 1)$ the quantum particle spreads ballistically in time as shown in Fig. 4(a). This is expected as the parameters values lie in the extended regime of the global phase diagram shown in Fig. 3(b). For $(t, \Delta) = (1.5, 1)$ shown in Fig. 4(b), the quantum particle spreads very slowly which is not visible on the time scale we have reported here. However, the particle is spread over several lattice sites. In the case of $(t, \Delta) = (0.3, 4)$, the quantum particle is strongly localized as probabilities are confined to the initial positions. The results of all three cases support the findings of the static analysis presented in the global phase diagram shown Fig. 3(b) for the case of $\phi = \phi_{rel.} = 0$.

To further support the findings of the static analysis with real-time transport of a quantum particle, we computed the dynamical IPR from the time evolved quantum state. For each pair of parameters (t, Δ) considered in Figs. 4(a)–(c), we started with a quantum state initially localized around a single site in the middle of the 1D lattice and evolved it for a longer period of time, i.e. $t_e = 1000$. This allows us to see the transient-time behavior as well as the steady state behavior of the dynamical IPR. In Figs. 4(d)–(f), we show our numerical results for $(t, \Delta) = (0.3, 1)$, $(t, \Delta) = (1.5, 1)$, and $(t, \Delta) = (0.3, 4)$, respectively. On a

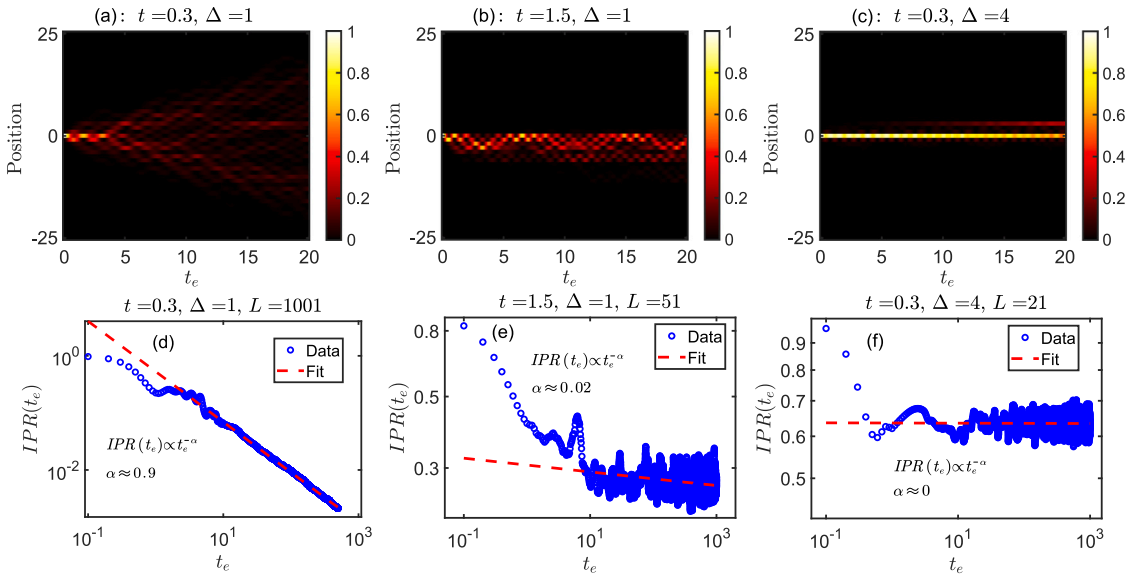

Fig. 4. (First row): Continuous-time quantum walks in the GAAH model under PBCs for three different values of the parameters pair (t, Δ) indicated for each panel. (a) The quantum particle spreads ballistically which is a signature of an extended phase. (b) the case of intermediate regime as the particle spreads slowly, and (c) the case of localized phase as the probabilities do not spread. (Second row): Dynamics of the IPR computed for the same set of parameters considered in (a)–(c). The estimated values of the critical exponent α of $1/t_e$ in each case (d)–(f) are indicated in the corresponding insets. All results are simulated with $\phi = 0$ and $\phi_{rel.} = 0$.

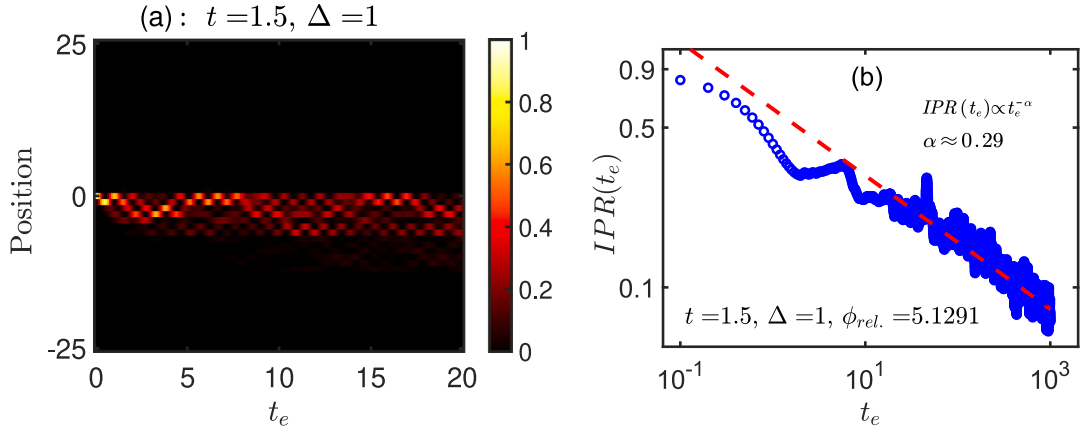

Fig. 5. (a) CTQW and (b) dynamics of IPR computed for (t, Δ) in the critical phase of the phase diagram for the $\phi_{rel} = 5.1291$ case shown in Fig. 3(e). As the critical phase is clearly separated from the extended and localized phases in this case, the IPR here decreases relatively faster with time ($\alpha \approx 0.29$) as compared to the case of $\phi_{rel.} = 0$ shown in Fig. 4(e) where α is ≈ 0.02.

log–log scale, the dynamical behavior of the IPR can be well captured by a power-law relation of the form

$$\mathrm{IPR}(t_e) \propto t_e^{-\alpha}.$$

In each case, we extract the critical exponent α of the inverse of the evolution time $1/t_e$ by fitting the power law relation to the data at longer times. For the results presented in Fig. 4(d), we get the critical exponent $\alpha \sim 0.9$. This shows that the IPR scales approximately linearly with $1/t_e$ (till it reaches its minimum value set by the finite size of the system). This shows that the quantum particle spreads ballistically, which is a signature of an extended phase. Fig. 4(e) shows that after an initial fast descent followed by transient-time oscillations at a shorter time scale ($t_e \sim 10^1$), the IPR decreases very slowly. The critical exponent in this case is $\alpha \sim 0.02$ which corresponds to a slow spreading of the particle. Similarly, in Fig. 4(e) the IPR reaches its steady-state value after an initial fast descent. The power-law fit in this case gives $\alpha \approx 0$ which characterizes a completely localized phase. These results of the dynamical IPR are consistent with the results of the static analysis presented in the phase diagram Fig. 3(b). This can be noticed by comparing both the values of IPR and the critical exponents ν and α in static and dynamics analyses, which agree perfectly.

For a nonzero $\phi_{rel.}$ case, we repeat the dynamical analysis only for a pair of parameters in the critical phase as the behavior of the extended and localized phases does not change with $\phi_{rel.}$. In Fig. 5, we report our numerical results for the evolution of a CTQW and the dynamical IPR. While the CTQW evolution does not show significant difference with the $\phi_{rel.} = 0$ case (on the reported time scale), the behavior of dynamical IPR clearly deviates from the extended and localized phases' behavior. This is quantitatively confirmed by a power law fitting that results in the critical exponent $\alpha \approx 0.29$. These results corroborate with the results presented in the phase diagram shown in Fig. 3(e).

CTQWs on the GAAH lattice with open ends

The GAAH model has topological properties, i.e. it hosts TE states on a lattice with open ends. Our results presented in Fig. 2 show

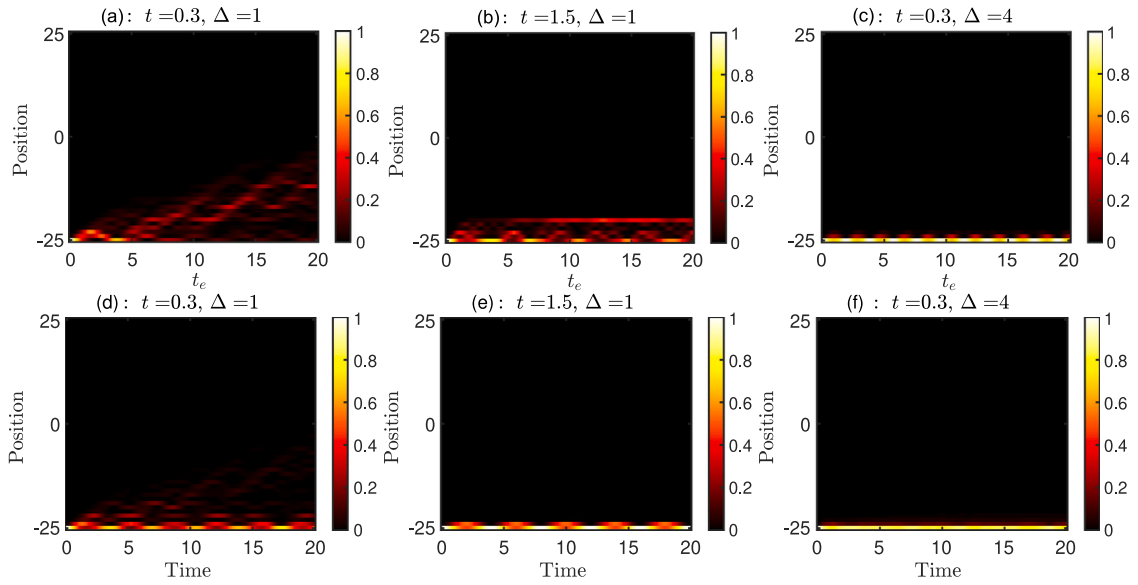

Fig. 6. First row: Continuous-time quantum walks dynamics in the GAAH lattice under OBCs with $\phi = 0$ so that the Hamiltonian hosts no TE states. The evolution of the CTQWs reflects the nature of (a) extended phase (b) intermediate regime, and (c) localized phase similar to the case of PBCs. Second row: we consider $\phi = 0.95\pi$ for (d) and (e) so that the GAAH hosts TE states which affect the spread of the quantum particle. (f) The probabilities shown are averaged over 50 values of ϕ in the range of 0 to 2π. These results are simulated with $\phi_{rel.} = 0$.

these states which are localized at the ends of the lattice. For a CTQW evolution, if we put a quantum particle at one of the two ends of the lattice, then the initial state will have a spatial overlap with the edge states. As a result, the evolution of the CTQW may not reflect the true nature of a phase corresponding to the chosen parameters (t, Δ). For example, (t, Δ) may be chosen from the extended phase or critical phase but the CTQW evolution will show that the quantum particle remains localized at the end of the lattice. In this case the localization will be due to the overlap of the initial state with TE states.

In Figs. 6, we show CTQWs evolution of a quantum particle initially localized at m=−25 under OBCs for the case of $\phi_{rel.} = 0$. As the energy spectrum in Figs. 2(a)–(c) shows that TE states exist only for certain values of ϕ. We study the evolution of a quantum particle for both cases, i.e., with and without TE states. In Figs. 6(a)–(c) we present our results for $\phi = 0$, for which the GAAH Hamiltonian hosts no TE states. As a result, the evolution of the quantum particle, for a given pair of parameters (t, Δ), is similar to the evolution in the case of periodic boundary conditions (PBCs). The results shown in Figs. 6(d)–(f) are simulated with the same parameters (t, Δ) values as used for the results shown in the first row of the figures, but with different values of ϕ. For example, the results shown in Figs. 6(d) and (e) are simulated with $\phi = 0.95\pi$. This ensures the existence of TE states at the ends of the lattice. Because of the non-zero overlap of the initial state, the spread of the CTQW is affected. For the parameters chosen from the extended phase, see Fig. 6(d), the quantum particle has a larger probability to remain localized than to spread. Similar is the case of Figs. 6(e) which shows complete localization despite the fact that (t, Δ) belongs to the intermediate regime. In both cases, the localization is due to the overlap of the initial state with the TE states. In Fig. 6(f), we show the evolution of a CTQW for (t, Δ) in the localized phase. The localization of the probabilities is independent of ϕ, that is, a quantum particle is localized regardless of the presence or absence of TE states.

Conclusion

In this work, we conducted a comprehensive study of the localization–delocalization transition in the one-dimensional generalized Aubry–André–Harper (GAAH) model in optical superlattice potentials using static and dynamical probes. Within the static analysis, we examined the single-particle energy spectrum as a function of the phase parameter ϕ for various values of t and Δ. In the extended phase, the GAAH model with OBCs exhibits delocalized bulk states along with topologically protected edge states localized at the lattice ends. In contrast, in the localized phase, the bulk states become confined to few lattice sites. To characterize this behavior, we employed the inverse participation ratio (IPR) as a diagnostic tool to distinguish between localized, extended, and critical phases, computing both state-resolved and averaged IPRs. This approach enabled us to identify the presence of mobility edges and to construct a global phase diagram in the $t - \Delta$ plane that highlights localized, extended, and critical phases.

For the dynamical analysis, we considered continuous-time quantum walks (CTQWs) of an initially localized particle. We evaluated the time-dependent probability distribution and the dynamical IPR. By analyzing the critical exponent α of the inverse evolution time $1/t_e$ of the dynamical IPR, we identified three distinct dynamical regimes in the phase diagram: extended, localized, and intermediate. Importantly, we observed a consistent correspondence between the static and dynamical results: phases identified as localized, extended, or critical through static IPR analysis exhibited transport behaviors that were in agreement with their spectral properties. Our findings provide a foundation for exploring the interplay between localization and topological phenomena in the GAAH model in optical superlattice potentials.

CRediT authorship contribution statement

Zain Ullah: Writing – original draft, Conceptualization. **Muhammad Sajid:** Writing – review & editing, Validation, Conceptualization. **Amsyar Rahim:** Writing – review & editing, Supervision. **Mohd Faudzi Umar:** Writing – review & editing, Supervision. **Nurisya Mohd Shah:** Writing – review & editing, Supervision, Investigation, Funding acquisition.

Declaration of competing interest

The authors declare that they have no known competing financial interests or personal relationships that could have appeared to influence the work reported in this paper.

Acknowledgment

NMS would like to acknowledge the grant, GP-UPM 9752900.

Data availability

Data will be made available on request.

References

[1] Sokoloff J. Unusual band structure, wave functions and electrical conductance in crystals with incommensurate periodic potentials. Phys Rep 1985;126(4):189–244, URL https://www.sciencedirect.com/science/article/pii/0370157385900882.
[2] Harper PG. The general motion of conduction electrons in a uniform magnetic field, with application to the diamagnetism of metals. Proc Phys Soc Lond Sect A 1955;68(10):879.
[3] Hofstadter DR. Energy levels and wave functions of Bloch electrons in rational and irrational magnetic fields. Phys Rev B 1976;14:2239–49.
[4] Aubry S, André G. Analyticity breaking and Anderson localization in incommensurate lattices. In: Ann. isr. phys. soc.. vol. 3, Israel Physical Society; 1980, p. 18.
[5] Longhi S. Metal-insulator phase transition in a non-hermitian Aubry-André-Harper model. Phys Rev B 2019;100:125157, URL https://link.aps.org/doi/10.1103/PhysRevB.100.125157.
[6] Longhi S. Phase transitions in a non-hermitian aubry-andré-harper model. Phys Rev B 2021;103:054203, URL https://link.aps.org/doi/10.1103/PhysRevB.103.054203.
[7] Sajid M, Shah M, Khan NA, Jan M. Quantum walks in an inhomogeneous off-diagonal Aubry-André-Harper model. Phys Lett A 2023;469:128763.
[8] Sajid M, Khan NA, Shah M. Topological pumping in an inhomogeneous Aubry-André model. Chinese J Phys 2024;92:311–20.
[9] Thouless DJ. Bandwidths for a quasiperiodic tight-binding model. Phys Rev B 1983;28:4272–6, URL https://link.aps.org/doi/10.1103/PhysRevB.28.4272.
[10] Kohmoto M. Metal-insulator transition and scaling for incommensurate systems. Phys Rev Lett 1983;51:1198–201, URL https://link.aps.org/doi/10.1103/PhysRevLett.51.1198.
[11] Izrailev FM. Simple models of quantum chaos: Spectrum and eigenfunctions. Phys Rev Lett 1986;56:541.
[12] Hiramoto H, Kohmoto M. New localization in a quasiperiodic system. Phys Rev Lett 1989;62:2714–7.
[13] Tang L, Thouless DJ. Diffusion and localization in an incommensurate potential. Phys Rev B 1992;45:103.
[14] Sil S, Maiti SK, Chakrabarti A. Metal-insulator transition in an aperiodic ladder network: An exact result. Phys Rev Lett 2008;101:076803, URL https://link.aps.org/doi/10.1103/PhysRevLett.101.076803.
[15] Li X, Pixley JH, Das Sarma S. Many-body localization in a quasiperiodic system. Phys Rev B 2018;97:245126.
[16] Yuan D, et al. Dynamics of localization-delocalization transition in quasiperiodic lattices. Phys Rev A 2019;99:043319.
[17] Rossignolo M, Dell'Anna L. Localization transitions and mobility edges in coupled Aubry-André chains. Phys Rev B 2019;99:054211, URL https://link.aps.org/doi/10.1103/PhysRevB.99.054211.
[18] Roy S, Ghosh S, Sen A. Interplay of interactions and quasiperiodic potential in a many-body localized system. Phys Rev Lett 2020;125:250402.
[19] Roy S, Mishra T, Tanatar B, Basu S. Reentrant localization transition in a quasiperiodic chain. Phys Rev Lett 2021;126:106803, URL https://link.aps.org/doi/10.1103/PhysRevLett.126.106803.
[20] Khan NA, Chen W, Jan M, Xianlong G. Linear-scale simulations of quench dynamics. Comput Phys Comm 2024;299:109132, URL http://dx.doi.org/10.1016/j.cpc.2024.109132.
[21] Ye S, Zhou Z, Khan NA, Xianlong G. Energy-dependent dynamical quantum phase transitions in quasicrystals. Phys Rev A 2024;109:043319, URL https://link.aps.org/doi/10.1103/PhysRevA.109.043319.
[22] Khan NA. Fidelity susceptibility probes of dynamical quantum criticality. Chaos Solitons Fractals 2024;183:114975.
[23] Ye S, Khan NA, Sajid M. Disentangling connection between static and dynamical phase transitions. Phys Rev A 2025;111:042208, URL https://link.aps.org/doi/10.1103/PhysRevA.111.042208.
[24] Anderson PW. Absence of diffusion in certain random lattices. Phys Rev 1958;109:1492.
[25] Santos Pires JP, Khan NA, Viana Parente Lopes JM, Lopes dos Santos JMB. Global delocalization transition in the de Moura–Lyra model. Phys Rev B 2019;99:205148, URL https://link.aps.org/doi/10.1103/PhysRevB.99.205148.
[26] Bloch I, Dalibard J, Zwerger W. Many-body physics with ultracold gases. Rev Modern Phys 2008;80:885–964.
[27] Lahini Y, Pugatch R, Pozzi F, Sorel M, Morandotti R, Davidson N, Silberberg Y. Observation of a localization transition in quasiperiodic photonic lattices. Phys Rev Lett 2009;103:013901.
[28] Sánchez-Palencia L, Lewenstein M. Disordered quantum gases under control. Nat Phys 2010;6:87.
[29] Kraus YE, Lahini Y, Ringel Z, Verbin M, Zilberberg O. Topological states and adiabatic pumping in quasicrystals. Phys Rev Lett 2012;109:106402, URL https://link.aps.org/doi/10.1103/PhysRevLett.109.106402.
[30] Verbin M, Zilberberg O, Kraus YE, Lahini Y, Silberberg Y. Observation of topological phase transitions in photonic quasicrystals. Phys Rev Lett 2013;110:076403, URL https://link.aps.org/doi/10.1103/PhysRevLett.110.076403.
[31] Schreiber M, Hodgman SS, Bordia P, Lü schen HP, Fischer MH, Vosk R, Altman E, Schneider U, Bloch I. Observation of many-body localization of interacting fermions in a quasirandom optical lattice. Science 2015;349:842–5.
[32] Kohlert T, Scherg S, Li X, Lüschen HP, Das Sarma S, Bloch I, Aidelsburger M. Observation of many-body localization in a one-dimensional system with a single-particle mobility edge. Phys Rev Lett 2019;122:170403, URL https://link.aps.org/doi/10.1103/PhysRevLett.122.170403.
[33] Ni X, Chen K, Weiner M, Apigo DJ, Prodan C, Alù A, Prodan E, Khanikaev AB. Observation of hofstadter butterfly and topological edge states in reconfigurable quasi-periodic acoustic crystals. Commun Phys 2019;2(1).
[34] An FA, Meier EJ, Gadway B. Observation of many-body localization in a one-dimensional quasiperiodic optical lattice. Phys Rev Lett 2021;126:040603.
[35] Liu F, Ghosh S, Chong YD. Localization and adiabatic pumping in a generalized aubry-andré-harper model. Phys Rev B 2015;91:014108, https://link.aps.org/doi/10.1103/PhysRevB.91.014108.
[36] Modugno M. Exponential localization in one-dimensional quasi-periodic structures. New J Phys 2009;11:033023.
[37] Ganeshan S, Pixley JH, Das Sarma S. Nearest neighbor tight binding models with an exact mobility edge in one dimension. Phys Rev Lett 2015;114:146601.
[38] Li X, Li X, Das Sarma S. Mobility edge and intermediate phase in the one-dimensional incommensurate lattice. Phys Rev B 2017;96:085119.
[39] Yuce C, Oztas Z. Generalized Aubry-André-Harper models. Phys Rev A 2019;99:062135.
[40] Wang H, et al. Two-dimensional generalizations of the Aubry-André model: Localization and topology. Phys Rev Lett 2020;125:196604.
[41] Khan NA, Ye S, Zhou Z, Cheng S, Xianlong G. Chebyshev polynomial approach to loschmidt echo: Application to quench dynamics in two-dimensional quasicrystals. Phys Rev E 2024;109:065311, URL https://link.aps.org/doi/10.1103/PhysRevE.109.065311.
[42] Zuo Z-W, Kang D. Reentrant localization transition in the su-schrieffer-heeger model with random-dimer disorder. Phys Rev A 2022;106:013305, URL https://link.aps.org/doi/10.1103/PhysRevA.106.013305.
[43] Lüschen HP, Scherg S, Kohlert T, Schreiber M, Bordia P, Li X, Das Sarma S, Bloch I. Single-particle mobility edge in a one-dimensional quasiperiodic optical lattice. Phys Rev Lett 2018;120:160404, URL https://link.aps.org/doi/10.1103/PhysRevLett.120.160404.
[44] An FA, Padavić K, Meier EJ, Hegde S, Ganeshan S, Pixley JH, Vishveshwara S, Gadway B. Interactions and mobility edges: Observing the generalized Aubry-André model. Phys Rev Lett 2021;126:040603.
[45] Li H, Wang Y-Y, Shi Y-H, Huang K, Song X, Liang G-H, Mei Z-Y, Zhou B, Zhang H, Zhang J-C, Chen S, Zhao SP, Tian Y, Yang Z-Y, Xiang Z, Xu K, Zheng D, Fan H. Observation of critical phase transition in a generalized Aubry-André-Harper model with superconducting circuits. Npj Quantum Inf 2023;9(1).
[46] Lin Q, Cedzich C, Zhou Q, Xue P. Observation of metal-insulator and spectral phase transitions in Aubry-André-Harper models. 2025, http://dx.doi.org/10.48550/ARXIV.2508.08255.
[47] Chang Y-J, Zhang J-H, Lu Y-H, Yang Y-Y, Mei F, Ma J, Jia S, Jin X-M. Observation of photonic mobility edge phases. Phys Rev Lett 2025;134:053601.
[48] Li Y, Zhang J-H, Mei F, Ma J, Xiao L, Jia S. Generalized Aubry-André-Harper models in optical superlattices. Chin Phys Lett 2022;39(6):063701.
[49] Konno N. Quantum walk note on the discrete-time quantum walk in one dimension. Quantum Inf Process 2002;1:345–54.
[50] Childs AM. Universal computation by quantum walk. Phys Rev Lett 2009;102:180501.
[51] An FA, Meier EJ, Gadway B. Realization of a continuous-time quantum walk with interacting fermions. Nat Commun 2017;8:325.
[52] Wegner F. Inverse participation ratio in $2+\epsilon$ dimensions. Z. Phys B: Condens Matter Quanta 1980;36(3):209–14.